TECHNICAL REPORT

HUMAN FACE-OFF: A NEW METHOD FOR MAPPING EVOLUTIONARY RATES ON THREE-DIMENSIONAL DIGITAL MODELS

by SILVIA CASTIGLIONE[1] (iD), MARINA MELCHIONNA[1] (iD), ANTONIO PROFICO[2] (iD), GABRIELE SANSALONE[3] (iD), MARIA MODAFFERI[1], ALESSANDRO MONDANARO[4] (iD), STEPHEN WROE[3] (iD), PAOLO PIRAS[5] (iD) *and* PASQUALE RAIA[1] (iD)

[1]Dipartimento di Scienze della Terra, dell'Ambiente e delle Risorse, Università di Napoli Federico II, 80126, Napoli, Italy; silvia.castiglione@unina.it, marina.melchionna@unina.it
[2]PalaeoHub, Department of Archaeology & Hull York Medical School, University of York, Heslington, UK
[3]Function, Evolution & Anatomy Research Lab, Zoology Division, School of Environmental & Rural Science, University of New England, NSW 2351, Armidale, Australia
[4]Dipartimento di Scienze della Terra, Università degli studi di Firenze, 50121, Firenze, Italy
[5]Via Romero Rodriguez Pereira, 00136, Rome, Italy

Abstract: Modern phylogenetic comparative methods allow us to estimate evolutionary rates of phenotypic change, how these rates differ across clades, and to assess whether the rates remained constant over time. Unfortunately, currently available phylogenetic comparative tools express the rate in terms of a scalar dimension, and do not allow us to determine rate variations among different parts of a single, complex phenotype, or chart realized rate variation directly onto the phenotype. We present a new method which allows the mapping of evolutionary rate variation directly onto three-dimensional phenotypes, informing on the direction and magnitude of trait change automatically. Implemented using the function *rate.map* embedded in the R package RRphylo, this method is based on phylogenetic ridge regression rate estimates. Since the latter represent ridge regression slopes, they possess sign and magnitude. In RRphylo, different rates are calculated for different districts of the phenotype, which can then be visualized directly onto the phenotype itself. We present the application of *rate.map* to the evolution of facial skeleton in Hominoidea, the primate clade inclusive of *Homo* and the greater apes (including living and fossil taxa). We found that the highly derived, unique shape of the face in modern humans evolved through rapid phenotypic changes affecting the nasal bones, the brow ridge and the maxillary region. The canine fossa, a facial feature unique to *Homo sapiens*, did not belong to a region of rapid phenotypic change, and could be seen as the by-product of midface evolution as suggested by previous studies.

Key words: evolutionary rates, *rate.map*, Hominoidea, RRphylo, digital model.

ESTIMATING the tempo and mode of evolution is key to understanding phenotypic change along lineages. A variety of phylogenetic comparative methods (PCMs) have been developed to this purpose and different tools are now available to estimate the rates of phenotypic trait change and the testing of different evolutionary scenarios (Butler & King 2004; O'Meara 2012). In the past few decades, it has also become possible to compute different rates and fit diverse evolutionary scenarios to different parts of the tree (O'Meara *et al.* 2006; Revell & Harmon 2008; Elliot & Mooers 2014; Smaers *et al.* 2016). However, most PCMs calculate the evolutionary rate as a measure of trait variance accumulation over time representing the global rate of phenotypic change for the whole trait or structure, which cannot be decomposed over any specific part of the phenotype under investigation. This hinders our understanding of whether different portions of a complex phenotype evolve at different rates, and in which direction. With univariate data, that change as scalars, this is still perfectly feasible. Yet with shape data global rates are uninformative regarding the direction of change as they do not offer the opportunity to determine how or whether different parts of the phenotype evolve along different lines and at different paces.

Here we use a novel PCM method, *RRphylo*, which applies phylogenetic ridge regression to estimate the evolutionary rate of phenotypic change for each branch of the tree, and calculates ancestral states in the process (Castiglione *et al.* 2020). Under *RRphylo*, rates are represented by phylogenetic ridge regression slopes estimated at the branches. Since slopes have a sign and a magnitude, it is possible to assess whether the phenotypic value increases or decreases, and at what speed, along the branches by looking at *RRphylo* rates alone (Price-Waldman *et al.* 2020). By performing *RRphylo* on PC scores retrieved from geometric morphometrics (GM) data analysis, which decomposes shape variation into orthogonal axes related to different portions of the phenotype, *RRphylo* rates can inform on whether PC scores values are increasing or decreasing, and how rapid these changes in value are. This is valuable because PC axes represent deformations of the reference mean shape which can be visualized. Consequently, computing *RRphylo* rates on PC scores offers the unique opportunity to visualize the direction and rate of change at specific locations of the phenotype, which cannot be achieved with any other PCM.

Here, we propose a new R function, named *rate.map*, embedded in the R package RRphylo v.2.5.7 (Castiglione *et al.* 2018), which allows the user to graphically visualize the tempo (rate) and direction (mode) of phenotypic change on anatomical structures of interest. *rate.map* works by identifying the PC axes linked to highest (and lowest) evolutionary rate values and reconstructs the morphology weighted on the selected PC axes. In this way, rather than using the evolutionary rate to assess the magnitude of global phenotypic change, users of *rate.map* can readily observe where and how the phenotype changed the most between any pair of taxa in the tree. Since *RRphylo* reconstructs phenotypes at nodes, *rate.map* can be used to compare either a species to a parental node, or pairs of species tracing back to their most recent common ancestor. In the present study we have applied the new *rate.map* function to chart evolutionary rates on the facial skeleton in apes including hominins. In the human lineage the face changed dramatically evolving from typically ape-like to the orthognatic and small-toothed condition seen in *Homo sapiens*.

MATERIAL AND METHOD

Data preparation

We worked on 42 triangular surface meshes of crania belonging to 12 extant and extinct species of ape (Hominoidea) (Castiglione *et al.* 2021). The living species include *Gorilla gorilla* (n = 4), *Homo sapiens* (n = 8), *Hylobates lar* (n = 6), *Pan troglodytes* (n = 5), *Pongo abelii* (n = 5), *Symphalangus syndactylus* (n = 5). The fossil species included were: *Australopithecus africanus* (Sts5; n = 1), *Homo habilis* (KNM-ER 1813; n = 1), *H. erectus* (Sangiran-17; n = 1), *H. heidelbergensis* (Kabwe I; Petralona; n = 2), *H. neanderthalensis* (Amud 1; Gibraltar 1; n = 2), *H. sapiens* (Skhul-V; n = 1) and *Paranthropus boisei* (KNM-ER 406; OH 5; n = 2). A full description of the fossil specimens is provided in Appendix S1. The digital meshes of the extant species other than *Homo sapiens* were taken from the Smithsonian Institute digital collection (https://humanorigins.si.edu/contact) and the Digital Morphology Museum (Kupri; http://dmm.pri.kyoto-u.ac.jp). Specimens of modern *H. sapiens* were downloaded from the NESPOS online database (https://www.nespos.org). Israel Hershkovitz and Julia Abramov kindly provided Amud 1 skull surfaces. Gibraltar 1, Sangiran-17, KNM-ER 1813, KNM-ER 406, Kabwe I and Petralona were kindly provided by Giorgio Manzi. The 3D model of Sts-5 was acquired from the virtual anthropology archive of the University of Vienna (https://www.virtual-anthropology.com/virtual-anthropology/share/digital-archive-of-fossil-hominoids/).

Some fossil specimens present distortions or missing parts due to taphonomic disturbance. The Neanderthal Gibraltar 1 skull lacks the left margin on the brow ridge and the zygomatic arch (Appendix S1: Fig. S1A). KNM-ER 1813 lacks the left maxillary and zygomatic bones, and the left orbit is markedly deformed (Appendix S1: Fig. S1B). The left zygomatic and maxillary bones of KNM-ER 406 are incomplete and covered by matrix (Appendix S1: Fig. S1C). We restored the missing parts by mirroring their undamaged counterparts. We first retrodeformed the cranium (*retroDeformMesh* function, Morpho R package v.2.8; Schlager 2017; Schlager *et al.* 2018, 2020). Then, we created a mirrored version of the symmetrized surface and then aligned them. Using Geomagic Studio software (2014), we selected the areas that needed to be restored and then merged these areas with the original model (for further information see Appendix S1: Fig. S1; Castiglione *et al.* 2021).

On each cranium we manually sampled 29 anatomical landmarks (Fig. 1, Table 1) by using Amira software (v.5.4.5; Visualization Sciences Group, ©2013). We defined 1000 surface semilandmarks (500 per side) which were slid by using the *slider3d* function included in the Morpho R package (Schlager 2017). As we were not interested in testing any sort of asymmetry, the bilateral semilandmark sets were symmetrized by using the *symmetrize* function in Morpho.

Procrustes superimposition and RRphylo

By applying *rate.map*, our goal was to chart evolutionary rates in the facial skeleton evolution of hominoids, inclusive of extinct human species. To filter out non-shape differences (rotation, position and size), we translated,
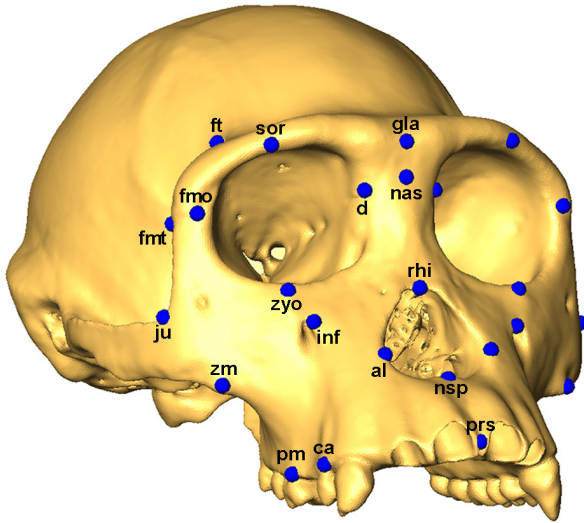
FIG. 1. Landmark configuration used in this study. Landmark abbreviations are explained in Table 1.

rotated and scaled the configurations via generalized Procrustes analysis (GPA; Gower 1975). We then performed a principal component analysis (PCA) on the aligned landmark's coordinates. We accomplished this procedure with the Morpho function *procSym* (Schlager 2017). This function returns both aligned coordinates and scores from the PCA. Using PC scores as shape information and a phylogeny inclusive of all species, we computed evolutionary rates by using the function *RRphylo* embedded in the RRphylo R package (Castiglione *et al.* 2018). The phylogeny of hominins is characterized by a stable topological arrangement with *H. sapiens* and *H. neanderthalensis* placed as sister species. Moving from this pair, from the least to the most inclusive clade, the tree includes *H. heidelbergensis*, *H. erectus*, *H. habilis*, the australopiths and eventually greater and lesser apes (Villmoare 2018; Diniz-Filho *et al.* 2019; Parins-Fukuchi *et al.* 2019; Püschel *et al.* 2021). Extinction dates represent the last appearance for each species: *A. africanus*, 2.03 Ma (Pickering *et al.* 2019); *H. habilis*, 1.6 Ma (de la Torre *et al.* 2021); *H. erectus*, 0.1 Ma (Rizal *et al.* 2020); *P. boisei*, 1.34 Ma (Dominiguez-Rodrigo *et al.* 2013); *H. heidelbergensis*, 224 ka (Lu *et al.* 2011; Arnold *et al.* 2015); *H. neanderthalensis*, 40 ka (Higham *et al.* 2014).
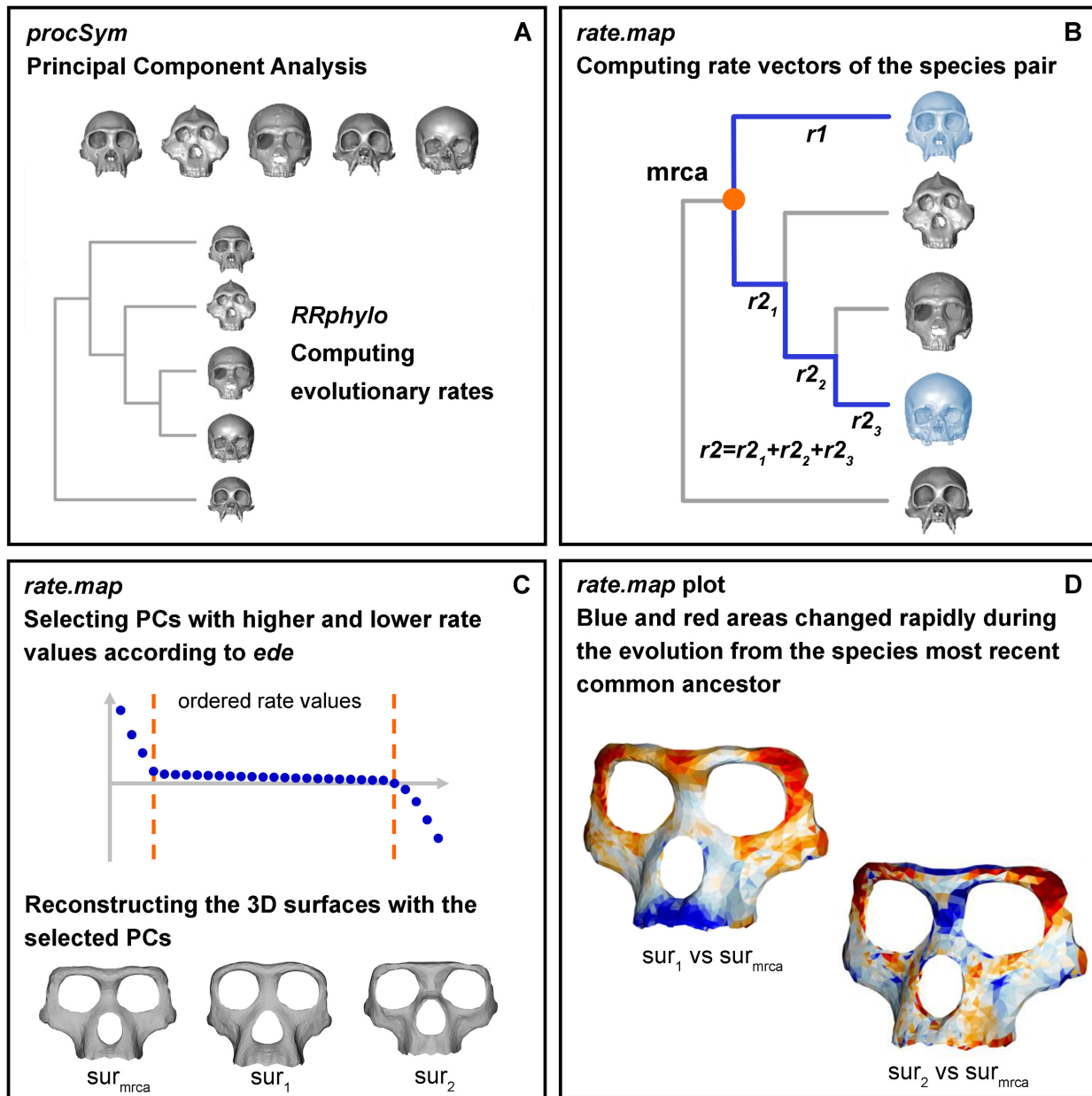
Mapping rates of shape evolution

The phenotype is summarized by the PC scores retrieved from the Procrustes superimposition and the PCA. For any two species in the tree, or for a species and any of its parental nodes, the function retrieves multivariate rates of phenotypic transformation (as many rates as the number

TABLE 1. Landmark descriptions and abbreviations.

N°	Landmark	Definition
1	Prosthion (prs)	Midline point at the most anterior point on the alveolar process of the maxillae
2	Nasospinale (nsp)	Lowest point of the inferior margin of the nasal aperture as projected on the mid-sagittal plane
3	Nasion (nas)	Midline point where the two nasal bones and the frontal intersect
4	Glabella (gla)	Midline bony prominence between the superciliary arches of the frontal bone, representing the most anterior part of the forehead looking straight ahead
5,6	Alare (al)	Most lateral point on the margin of the anterior nasal aperture
7,8	Zygoorbitale (zyo)	Point at which the orbital rim intersects the zygomaticomaxillary suture
9,10	Frontomalare orbitale (fmo)	Point at which the frontozygomatic suture crosses the inner orbital rim
11,12	Frontomalare temporale (fmt)	Point at which the frontozygomatic suture crosses the temporal line
13,14	Dacryon (d)	Point at which the maxillolacrimal suture meets the frontal bone
15,16	Zygomaxillare (zm)	Most inferior point on the zygomaticomaxillary suture
17	Rhinion (rhi)	Midline point at the inferior free end of the internasal suture
18,19	Jugale (ju)	Notch between the temporal and frontal processes of the zygomatic
20,21	Infraorbital foramen (inf)	Upper margin of the infraorbital foramen
22,23	Canine (ca)	External alveolar margin of the canine
24,25	Premolar (pm)	External alveolar margin of the second premolar
26,27	Superior orbital (sor)	Highest point on the orbital margin
28,29	Frontotemporal constriction (ft)	Point of narrowing of the cranium just behind the eye sockets

Landmark definition from White *et al.* (2011).

of PCs) from an *RRphylo* object (Fig. 2A–B, Table 2). Given an ancestor–descendant pair within the tree, the phenotypic difference between them is defined by the sum of subsequent changes occurring along the path leading to the species. The amount of shape change is thus described by the algebraic sum of the evolutionary rate values computed along all the branches occurring in between the ancestor and the descendant, separately for each PC score, giving a vector r of rate sums of length n (the number of PCs). For any pair of species, the resulting multivariate rate vectors (r_1, r_2) describing the shape

FIG. 2. Graphical representation of the *rate.map* function workflow. A, the morphological information (obtained with *procSym* function in Morpho), and the evolutionary rates (computed with *RRphylo* function in RRphylo) are the initial data. B, for each indicated species/node, *rate.map* (RRphylo) computes the rate vectors (i.e. the sum of all rates along the evolutionary path from the species/nodes to the most recent common ancestor). C, the rate vectors are ordered; the highest and lowest vectors are selected in relation of the inflection points; the associated PCs are selected and used to reconstruct the surfaces of the two species/nodes (***sur_1*** and ***sur_2***), and that of the most recent common ancestor (***sur_mrca***). D, *rate.map* displays the local area comparison in terms of expansion (blue triangles) or contraction (red triangles) between each surface and the most recent common ancestor of the species pair (mrca).

change from each species in the pair to their common ancestor, are separately inspected for inflection points to identify those PC axes associated with the greatest phenotypic change (i.e. the largest summed rate values; Fig. 2B). The inflection points are identified by using the function *ede* in the R package inflection (Christopoulos 2019). *ede*

performs an extreme distance estimator (Christopoulos 2012, 2016) to efficiently locate the inflection points along a curve. We used the identified PC axes along each (r_1 and r_2) vector, and their associated loadings, to estimate the landmark configurations for the analysed species/nodes pair by using the *showPC* Morpho function

TABLE 2. Explanation of *rate.map* arguments.

Argument name	Explanation
x	The species/nodes to be compared; it can be a single species, or a vector containing two species, or a species and a node to be compared
RR	An object generated by using the *RRphylo* function
PCscores	PC scores
pcs	PC vectors of all the samples
mshape	The consensus configuration
out.rem	Logical: if TRUE triangles with outlying area difference are removed
shape.diff	Logical: if TRUE, the mesh area differences are displayed in a second 3D plot
show.names	Logical: if TRUE, the names of the species are displayed in the 3D plot

(v.2.8). In this way, the new configurations are weighted based on the most significant amount of shape change, discarding minor shape variation. Starting from the new configurations, the function automatically reconstructs the new 3D surfaces (*sur₁*, *sur₂*) associated with the selected PC axes, using the ball-pivoting algorithm (Bernardini *et al.* 1999) implemented in the function *vcgBallPivoting* in the R package Rvcg (Schlager 2017). The same procedure is used to reconstruct the landmark configuration and the 3D surfaces of the most recent common ancestor (*sur$_{mrca}$*) between the analysed species/nodes without selecting any PCs (Fig. 2C). *sur₁* and *sur₂* are both compared with *sur$_{mrca}$* using the algorithm embedded in the *localmeshdiff* function of the Arothron R package (Profico *et al.* 2021). *localmeshdiff* compares the area differences between corresponding triangles of each 3D surfaces and *sur$_{mrca}$*. As a final product, *rate. map* automatically returns a 3D plot showing the two comparisons (*sur₁* against *sur$_{mrca}$*, and *sur₂* against *sur$_{mrca}$*) displayed on *sur$_{mrca}$* (Table 3). This procedure effectively illustrates the direction and magnitude of phenotypic change for any pair of species in reference to their most recent common ancestor. The colour gradient goes from blue to red, where blue areas represent expansion of the mesh (compared to *sur$_{mrca}$*) and red areas represent contractions of the mesh triangles (Fig. 2D).

TABLE 3. Explanation of *rate.map* returned values.

Value	Explanation
Selected	List of PC axes selected for higher evolutionary rates for each species
Surfaces	List of reconstructed coloured surfaces of the given species and of the most recent common ancestor

rate.map further allows us to investigate the pure morphological comparison of shapes by excluding the evolutionary rate component. By setting the argument *show.diff* = TRUE, *sur₁* and *sur₂* will be reconstructed without selecting any PC axes and compared one against the other. In this case, a second 3D plot will be displayed highlighting area differences in terms of expansion (green) and contraction (yellow) (Appendix S1, Fig. S2).

RESULTS

We show *rate.map* results for three different comparisons: *H. sapiens* – *H. neanderthalensis* (Fig. 3A), *H. sapiens* – *H. erectus* (Fig. 3B) and *H. sapiens* – *A. africanus* (Fig. 3C). In all cases the reference surface is their respective *sur$_{mrca}$*. The first comparison is between sister species, the two others between different lineages with progressively deeper common ancestry.

From the comparison between *H. sapiens* and *H. neanderthalensis* it is clear that the brow ridges, and nasal regions changed very rapidly from those of their most recent common ancestor (mrca; Fig. 3A). *Homo sapiens* (left side) exhibits a restriction in the nasal area with a strong contraction of the brow ridge, and a narrow piriform aperture. Conversely, *H. neanderthalensis* (right side) developed an enlarged nasal cavity. Opposing patterns of evolution are also highlighted for the zygomatic bone. The midface of *H. neanderthalensis* is slightly more prognathic, a feature which is often reported in literature (Stelzer *et al.* 2018).

Figure 3B shows the comparison between *H. sapiens* and *H. erectus*. Relative to their most recent common ancestor, the lineage leading to *H. sapiens* shows a great reduction in the brow ridge and narrowing of the upper facial skeleton. Interestingly, brow ridge evolution in the lineage leading from the most recent common ancestor to *H. erectus* does not show high evolutionary rates, in keeping with the observation that this ancestor had a prominent brow.

Figure 3C shows the comparison of *H. sapiens* and *A. africanus* to their mrca (on the left and right, respectively). In *H. sapiens* a rapid forward expansion of the nasal bones and a thinning of the brow ridge are evident, and the dental arch appears reduced and laterally compressed.

DISCUSSION

In apes (Hominoidea), facial morphology plays a central role in recognition, communication and expression of emotions (Du *et al.* 2014; Lacruz *et al.* 2019). Craniofacial bones appear to be highly integrated with the brain case (Bastir & Rosas 2005; Marcucio *et al.* 2011) and to a lesser degree with the cranial base (Profico *et al.* 2017;
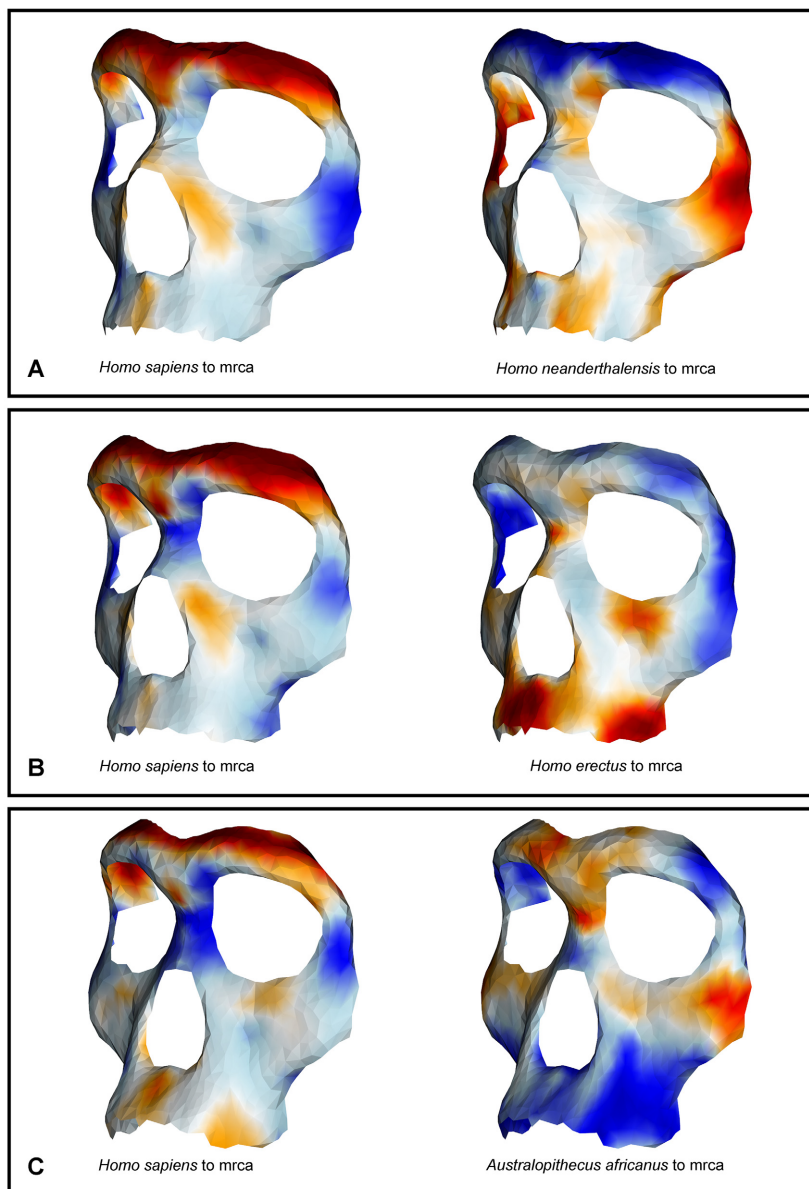
FIG. 3. Visualization of the pairwise comparison between *Homo sapiens* and: A, *H. neanderthalensis*; B, *H. erectus*; C, *Australopithecus africanus*. In each case, the left image shows the reconstructed surfaces of the last common ancestor (mrca) of *H. sapiens* and the comparator taxon using the PC axes related to the highest evolutionary rates for *H. sapiens*. On the right, we used the highest evolutionary rates for the comparator taxon. The colour gradient goes from blue (expanded areas) to red (contracted areas) and indicates the areas of the surfaces that changed at higher evolutionary rates during the evolution from the common ancestor.

Neaux *et al.* 2019). The shape of neurocranium and cranial base changed greatly in the course of human evolution. This is likely to be the consequence of long-term trends toward increased brain size and the acquisition of bipedalism (Masao *et al.* 2016). Yet, they are frequently interpreted as adaptations to different diets as well. Early representatives of the human lineage (i.e. *Australopithecus* and *Paranthropus*) may show a range of derived craniodental and osteological features conferring adaptation to hard food consumption (Teaford & Ungar 2000; Strait *et al.* 2009). However, this hypothesis has been challenged in recent years, as both functional, morphological and isotopic studies seem to point to less mechanically resistant food items as typical of most hominins (Grine *et al.*

2010; Cerling *et al.* 2011; Ungar *et al.* 2011; Delezene *et al.* 2013; Ledogar *et al.* 2016; Marcé-Nogué *et al.* 2020).

In general terms, living greater apes are characterized by marked prognathism, with long snouts and vertically deep faces. Conversely, fossils belonging to the human lineage present shorter midfaces with a vertical profile and follow an overall trend toward gracilization, but they still show a slightly prognathic premaxillary region common to the basal hominin species (Stelzer *et al.* 2018; Lacruz *et al.* 2019).

In the *H. sapiens* – *A. africanus* comparison, these patterns are readily evident. Reduced prognathism as well as thinning and outward expansion of the nasals have

evolved faster than other regions of the facial skull in *H. sapiens*. When compared to the inferred shape of their most recent common ancestor, rates of shape change in the *H. sapiens – H. neanderthalensis* pair are similarly evident. Modern humans rapidly developed a thinner brow ridge and nasals relative to Neanderthals, although well-developed brows are present in early representatives of our species from Jebel Irhoud, Herto and Skhul (Stringer 2016; Hublin *et al.* 2017). A less macroscopic, yet potentially more interesting pattern of phenotypic change occurs in the area around the canine fossa. In Neanderthals, this region is inflated, whereas a depression referred to as the canine fossa is present in *H. sapiens*. This pattern of change was attributed to bone remodelling during ontogeny in Schuh *et al.* (2019), but considered to be a by-product of the formation of surrounding structures, in keeping with Maddux & Franciscus (2009) and Freidline *et al.* (2012).

However, the reconstruction performed by *rate.map* indicates that the area of the canine fossa has been affected by slower rates of change than have surrounding regions; the nasal region in particular. This is consistent with the 'spandrel-like' hypothesis (*sensu* Gould & Lewontin 1979) of evolution of the canine fossa within a broader context of midface reorganization (Martinez-Maza *et al.* 2010).

CONCLUSION

Phenotypic evolutionary rates in *RRphylo* are estimated as phylogenetic ridge regression slopes. With shape data, this implies that each rate represents the magnitude and direction of shape change attached to specific PC axes, that is, to specific regions of the morphology of interest. This offers the unique opportunity to chart the rates on the phenotype, illustrating how and to what degree the phenotype changed over the course of evolution within an explicit phylogenetic context. We developed the function *rate.map* to compute and map such patterns of shape changes directly onto the phenotype. Applying this methodology to the evolution of the human lineage we find that the familiar morphology of the modern human face, with thin brow ridge and outwardly oriented, narrow nasal bones was the product of rapid evolution. Interestingly, the region of the canine fossa evolved slowly, in keeping with previous findings pointing to this feature as a by-product of adaptive changes in the surrounding regions of the midface.

Author contributions. SC and MMel equally contributed to this study. SC, MMel, AP, GS and PR conceived the study. SC, MMel, AM and PR produced the code. All the authors participated in writing the paper.

DATA AVAILABILITY STATEMENT

Data for this study are available in the Dryad Digital Repository: https://doi.org/10.5061/dryad.3n5tb2rhf

Editor. Philip Mannion

SUPPORTING INFORMATION

Additional Supporting Information can be found online (https://doi.org/10.1111/pala.12582):

Appendix S1. Supplementary material and results including descriptions of the material examined, phylogenetic tree in Newick format; also:

Table S1. List of the specimens used in the study.

Fig. S1. Restoration of: A, Gibraltar 1; B, KNM-ER 1813; C, KNM-ER 406.

Fig. S2. Pure morphological comparison of shapes obtained by setting the *rate.map* argument *show.diff* = TRUE.

Fig. S3. Multiple comparisons between species belonging to the Hominini (great apes).

data.RDA Data used in the manuscript, any relevant information can be found in the script file.

script.R Script written to perform the analyses in the R software environment.

REFERENCES

ARNOLD, L. J., DEMURO, M., PARÉS, J. M., PÉREZ-GONZÁLEZ, A., ARSUAGA, J. L., BERMÚDEZ DE CASTRO, J. M. and CARBONELL, E. 2015. Evaluating the suitability of extended-range luminescence dating techniques over early and Middle Pleistocene timescales: published datasets and case studies from Atapuerca, Spain. *Quaternary International*, **389**, 167–190.

BASTIR, M. and ROSAS, A. 2005. Hierarchical nature of morphological integration and modularity in the human posterior face. *American Journal of Physical Anthropology*, **128**, 26–34.

BERNARDINI, F., MITTLEMAN, J., RUSHMEIER, H., SILVA, C. and TAUBIN, G. 1999. The ball-pivoting algorithm for surface reconstruction. *IEEE Transactions on Visualization & Computer Graphics*, **5** (4), 349–359.

BUTLER, M. A. and KING, A. A. 2004. Phylogenetic comparative analysis: a modeling approach for adaptive evolution. *The American Naturalist*, **164**, 683–695.

CASTIGLIONE, S., TESONE, G., PICCOLO, M., MELCHIONNA, M., MONDANARO, A., SERIO, C., DI FEBBRARO, M. and RAIA, P. 2018. A new method for

testing evolutionary rate variation and shifts in phenotypic evolution. *Methods in Ecology & Evolution*, **9**, 974–983.

CASTIGLIONE, S., SERIO, C., MONDANARO, A., MELCHIONNA, M., CAROTENUTO, F., DI FEBBRARO, M., PROFICO, A., TAMAGNINI, D. and RAIA, P. 2020. Ancestral state estimation with phylogenetic ridge regression. *Evolutionary Biology*, **47** (3), 220–232.

CASTIGLIONE, S., MELCHIONNA, M., PROFICO, A., SANSALONE, G., MODAFFERI, M., MONDANARO, A., WROE, S., PIRAS, P. and RAIA, P. 2021. Data from: human face-off: a new method for mapping evolutionary rates on three-dimensional digital models. Dryad Digital Repository. https://doi.org/10.5061/dryad.3n5tb2rhf

CERLING, T. E., MBUA, E., KIRERA, F. M., MANTHI, F. K., GRINE, F. E., LEAKEY, M. G., SPONHEIMERE, M. and UNO, K. T. 2011. Diet of *Paranthropus boisei* in the early Pleistocene of East Africa. *Proceedings of the National Academy of Sciences*, **108** (23), 9337–9341.

CHRISTOPOULOS, D. T. 2012. Developing methods for identifying the inflection point of a convex/concave curve. arXiv preprint arXiv:1206.5478. https://arxiv.org/abs/1206.5478

CHRISTOPOULOS, D. T. 2016. On the efficient identification of an inflection point. *International Journal of Mathematics & Scientific Computing*, **6** (1), 2231–5330.

CHRISTOPOULOS, D. T. 2019. inflection: Finds the Inflection Point of a Curve. R package v.1.3.5. https://cran.r-project.org/package=inflection

TORRE, I. DE LA, BENITO-CALVO, A., MARTÍN-RAMOS, C., MCHENRY, L. J., MORA, R., JACKSON, K. N., PANTE, M. C., STANISTREETH, I. J. and STOLLHOFENK, H. 2021. New excavations in the MNK Skull site, and the last appearance of the Oldowan and *Homo habilis* at Olduvai Gorge, Tanzania. *Journal Anthropological Archaeology*, **61**, 101255.

DELEZENE, L. K., ZOLNIERZ, M. S., TEAFORD, M. F., KIMBEL, W. H., GRINE, F. E. and UNGAR, P. S. 2013. Premolar microwear and tooth use in *Australopithecus afarensis*. *Journal Human Evolution*, **65**, 282–293.

DINIZ-FILHO, J. A. F., JARDIM, L., MONDANARO, A. and RAIA, P. 2019. Multiple components of phylogenetic non-stationarity in the evolution of brain size in fossil hominins. *Evolutionary Biology*, **46** (1), 47–59.

DOMÍNGUEZ-RODRIGO, M., PICKERING, T. R., BAQUEDANO, E., MABULLA, A., MARK, D. F., MUSIBA, C., BUNN, H. T., URIBELARREA, D., SMITH, V., DIEZ-MARTIN, F., PÉREZ-GONZÁLEZ, A., SÁNCHEZ, P., SANTONIA, M., BARBONI, D., GIDNA, A., ASCHLEY, G., YRAVEDRA, J., HEATON, J. L. and ARRIAZA, M. C. 2013. First partial skeleton of a 1.34-million-year-old *Paranthropus boisei* from Bed II, Olduvai Gorge, Tanzania. *PLoS One*, **8** (12), e80347.

DU, S., TAO, Y. and MARTINEZ, A. M. 2014. Compound facial expressions of emotion. *Proceedings of the National Academy of Sciences*, **111** (15), E1454–E1462.

ELLIOT, M. G. and MOOERS, A. O. 2014. Inferring ancestral states without assuming neutrality or gradualism using a stable model of continuous character evolution. *BMC Evolutionary Biology*, **14**, 226.

FREIDLINE, S. E., GUNZ, P., HARVATI, K. and HUBLIN, J. J. 2012. Middle Pleistocene human facial morphology in an evolutionary and developmental context. *Journal of Human Evolution*, **63**, 723–740.

GRINE, F. E., JUDEX, S., DAEGLING, D. J., OZCIVICI, E., UNGAR, P. S., TEAFORD, M. F., SPONHEIMER, M., SCOTT, J., SCOTT, R. S. and WALKER, A. 2010. Craniofacial biomechanics and functional and dietary inferences in hominin paleontology. *Journal of Human Evolution*, **58**, 293–308.

GOULD, S. J. and LEWONTIN, R. C. 1979. The spandrels of San Marco and the Panglossian paradigm: a critique of the adaptationist programme. *Proceedings of the Royal Society B*, **205** (1161), 581–598.

GOWER, J. C. 1975. Generalized procrustes analysis. *Psychometrika*, **40**, 33–51.

HIGHAM, T., DOUKA, K., WOOD, R., RAMSEY, C. B., BROCK, F., BASELL, L., CAMPS, M., ARRIZABAL-AGA, A., BAENA, J., BARROSO-RUÍZ, C., BERGMAN, C., BOITARD, C., BOSCATO, P., CAPARRÓS, M., CONARD, N. J., DRAILY, C., FROMENT, A., GALVÁN, B., GAMBASSINI, P., GARCIA-MORENO, A., GRIMALDI, S., HAESAERTS, P., HOLT, B., IRIARTE-CHIAPUSSO, M.-J., JELINEK, A., PARDO, J. F. J., MAÍLLO-FERNÁNDEZ, J.-M., MAROM, A., MAROTO, J., MENÉNDEZ, M., METZ, L., MORIN, E., MORONI, A., NEGRINO, F., PANAGOPOULOU, E., PERESANI, M., PIRSON, S., DE LA RASILLA, M., RIEL-SALVATORE, J., RONCHITELLI, A., SANTA-MARIA, D., SEMAL, P., SLIMAK, L., SOLER, J., SOLER, N., VILLALUENGA, A., PINHASI, R. and JACOBI, R. 2014. The timing and spatiotemporal patterning of Neanderthal disappearance. *Nature*, **512** (7514), 306–309.

HUBLIN, J. J., BEN-NCER, A., BAILEY, S. E., FREIDLINE, S. E., NEUBAUER, S., SKINNER, M. M., BERGMANN, I., LE CABEC, A., BENAZZI, S., HARVATI, K. and GUNZ, P. 2017. New fossils from Jebel Irhoud, Morocco and the pan-African origin of *Homo sapiens*. *Nature*, **546** (7657), 289–292.

LACRUZ, R. S., STRINGER, C. B., KIMBEL, W. H., WOOD, B., HARVATI, K., O'HIGGINS, P., BROMAGE, T. G. and ARSUAGA, J. L. 2019. The evolutionary history of the human face. *Nature Ecology & Evolution*, **3** (5), 726–736.

LEDOGAR, J. A., SMITH, A. L., BENAZZI, S., WEBER, G. W., SPENCER, M. A., CARLSON, K. B., MCNULTY, K., DECHOW, P. C., GROSSE, I. R., ROSS, C. F., RICHMOND, B. G., WRIGHT, B. W., WANG, Q., BYRON, C., CARLSON, K. J., DE RUITER, D. J., BERGER, L. R., TAMVADA, K., PRYOR, L. C., MICHAEL, A., BERTHAUME, M. A. and STRAIT, D. S. 2016. Mechanical evidence that *Australopithecus sediba* was limited in its ability to eat hard foods. *Nature Communications*, **7**, 10596.

LU, Z., MELDRUM, D. J., HUANG, Y., HE, J. and SARMIENTO, E. E. 2011. The Jinniushan hominin pedal skeleton from the late Middle Pleistocene of China. *Homo*, **62** (6), 389–401.

MADDUX, S. D. and FRANCISCUS, R. G. 2009. Allometric scaling of infraorbital surface topography in *Homo*. *Journal of Human Evolution*, **56**, 161–174.

MARCÉ-NOGUÉ, J., PÜSCHEL, T. A., DAASCH, A. and KAISER, T. M. 2020. Broad-scale morpho-functional traits of the mandible suggest no hard food adaptation in the hominin lineage. *Scientific Reports*, **10** (1), 1–11.

MARCUCIO, R. S., YOUNG, N. M., HU, D. and HALL-GRIMSSON, B. 2011. Mechanisms that underlie co-variation of the brain and face. *Genesis*, **49**, 177–189.

MARTINEZ-MAZA, C., ROSAS, A. and NIETO-DIAZ, M. 2010. Brief communication: identification of bone formation and resorption surfaces by reflected light microscopy. *American Journal of Physical Anthropology*, **143**, 313–320.

MASAO, F. T., ICHUMBAKI, E. B., CHERIN, M., BARILI, A., BOSCHIAN, G., IURINO, D. A., MENCONERO, S., MOGGI-CECCHI, J. and MANZI, G. 2016. New footprints from Laetoli (Tanzania) provide evidence for marked body size variation in early hominins. *eLife*, **5**, e19568.

NEAUX, D., WROE, S., LEDOGAR, J. A., HEINS LEDOGAR, S. and SANSALONE, G. 2019. Morphological integration affects the evolution of midline cranial base, lateral basicranium, and face across primates. *American Journal of Physical Anthropology*, **170** (1), 37–47.

O'MEARA, B. C. 2012. Evolutionary inferences from phylogenies: a review of methods. *Annual Review of Ecology, Evolution, & Systematics*, **43**, 267–285.

O'MEARA, B. C., ANÉ, C., SANDERSON, M. J. and WAINWRIGHT, P. C. 2006. Testing for different rates of continuous trait evolution using likelihood. *Evolution*, **60** (5), 922–933.

PARINS-FUKUCHI, C., GREINER, E., MACLATCHY, L. M. and FISHER, D. C. 2019. Phylogeny, ancestors, and anagenesis in the hominin fossil record. *Paleobiology*, **45** (2), 378–393.

PICKERING, R., HERRIES, A. I., WOODHEAD, J. D., HELLSTROM, J. C., GREEN, H. E., PAUL, B., RITZMAN, T., STRAIT, D. S., SCHOVILLE, B. J. and HANCOX, P. J. 2019. U–Pb-dated flowstones restrict South African early hominin record to dry climate phases. *Nature*, **565** (7738), 226–229.

PRICE-WALDMAN, R. M., SHULTZ, A. J. and BURNS, K. J. 2020. Speciation rates are correlated with changes in plumage color complexity in the largest family of songbirds. *Evolution*, **74** (6), 1155–1169.

PROFICO, A., PIRAS, P., BUZI, C., DI VINCENZO, F., LATTARINI, F., MELCHIONNA, M., VENEZIANO, A., RAIA, P. and MANZI, G. 2017. The evolution of cranial base and face in Cercopithecoidea and Hominoidea: modularity and morphological integration. *American Journal of Primatology*, **79** (12), e22721.

PROFICO, A., BUZI, C., CASTIGLIONE, S., MELCHIONNA, M., PIRAS, P., VENEZIANO, A. and RAIA, P. 2021. Arothron: an R package for geometric morphometric methods and virtual anthropology applications. *American Journal of Physical Anthropology*, **176** (1), 144–151.

PÜSCHEL, H. P., BERTRAND, O. C., O'REILLY, J. E., BOBE, R. and PÜSCHEL, T. A. 2021. Divergence-time

estimates for hominins provide insight into encephalization and body mass trends in human evolution. *Nature Ecology & Evolution*, **5** (6), 808–819.

REVELL, L. J. and HARMON, L. J. 2008. Testing quantitative genetic hypotheses about the evolutionary rate matrix for continuous characters. *Evolutionary Ecology Research*, **10** (3), 311–331.

RIZAL, Y., WESTAWAY, K. E., ZAIM, Y., VAN DEN BERGH, G. D., BETTIS, E. A. III, MORWOOD, M. J., HUFFMAN, O. F., GRÜN, R., JOANNES-BOYAU, R., BAILEY, R. M., OETOMO, S. B., WESTAWAY, M. C., KURNIAWAN, I., MOORE, M. W., STOREY, M., AZIZ, F., SUMINTO, ZHAO, J.-X., ASWAN, SIPOLA, M. E., LARICK, R., ZONNEVELD, J.-P., SCOTT, R., PUTT, S. and CIOCHON, R. L. 2020. Last appearance of *Homo erectus* at Ngandong, Java, 117,000–108,000 years ago. *Nature*, **577**, 381–385.

SCHLAGER, S. 2017. Morpho and Rvcg – shape analysis in R: R-packages for geometric morphometrics, shape analysis and surface manipulations. 217-256. *In* ZHENG, G., LI, S. and SZÉKELY, G. (eds). *Statistical shape and deformation analysis: Methods, implementation and applications*. Academic Press, 508 pp.

SCHLAGER, S., PROFICO, A., DI VINCENZO, F. and MANZI, G. 2018. Retrodeformation of fossil specimens based on 3D bilateral semi-landmarks: implementation in the R package "Morpho". *PLoS One*, **13**, e0194073.

SCHLAGER, S., JEFFERIS, G. and DRYDEN, I. 2020. Morpho: Calculations and Visualisations Related to Geometric Morphometrics. R-package v.2.8. https://cran.r-project.org/web/packages/Morpho/index.html

SCHUH, A., KUPCZIK, K., GUNZ, P., HUBLIN, J. J. and FREIDLINE, S. E. 2019. Ontogeny of the human maxilla: a study of intra-population variability combining surface bone histology and geometric morphometrics. *Journal of Anatomy*, **235** (2), 233–245.

SMAERS, J. B., MONGLE, C. S. and KANDLER, A. 2016. A multiple variance Brownian motion framework for estimating variable rates and inferring ancestral states. *Biological Journal of the Linnean Society*, **118**, 78–94.

STELZER, S., NEUBAUER, S., HUBLIN, J.-J., SPOOR, F. and GUNZ, P. 2018. Morphological trends in arcade shape and size in Middle Pleistocene *Homo*. *American Journal of Physical Anthropology*, **168** (1), 70–91.

STRAIT, D. S., WEBER, G. W., NEUBAUER, S., CHALK, J., RICHMOND, B. G., LUCAS, P. W., SPENCER, M. A., SCHREIN, C., DECHOW, P. C., ROSS, C. F., GROSSE, I. R., WRIGHT, B. W., CONSTANTINO, P., WOOD, B. A., LAWN, B., HYLANDER, W. L., WANG, Q., BYRON, C., SLICE, D. E. and SMITH, A. L. 2009. The feeding biomechanics and dietary ecology of *Australopithecus africanus*. *Proceedings of the National Academy of Sciences*, **106**, 2124–2129.

STRINGER, C. 2016. The origin and evolution of *Homo sapiens*. *Philosophical Transactions of the Royal Society B*, **371** (1698), 20150237.

TEAFORD, M. F. and UNGAR, P. S. 2000. Diet and the evolution of the earliest human ancestors. *Proceedings of the National Academy of Sciences*, **97**, 13506–13511.

UNGAR, P. S., KRUEGER, K. L., BLUMENSCHINE, R. J., NJAU, J. and SCOTT, R. S. 2011. Dental microwear texture analysis of hominins recovered by the Olduvai Landscape Paleoanthropology Project, 1995–2007. *Journal of Human Evolution*, **63**, 429–437.

VILLMOARE, B. 2018. Early Homo and the role of the genus in paleoanthropology. *American Journal of Physical Anthropology*, **165**, 72–89.

WHITE, T. D., BLACK, M. T. and FOLKENS, P. A. 2011. *Human osteology*. Third edition. Academic Press. 688 pp.